PAPER • OPEN ACCESS

Electrical conductivity enhancement of transparent silver nanowire films on temperature-sensitive flexible substrates using intense pulsed ion beam

To cite this article: Marat Kaikanov *et al* 2021 *Nanotechnology* **32** 145706

View the article online for updates and enhancements.

Electrical conductivity enhancement of transparent silver nanowire films on temperature-sensitive flexible substrates using intense pulsed ion beam

Marat Kaikanov[1,2], **Aidar Kemelbay**[1] ⓘ, **Bauyrzhan Amanzhulov**[2], **Gulzat Demeuova**[2], **Gulnur Akhtanova**[1], **Farabi Bozheyev**[1,2] **and Alexander Tikhonov**[1] ⓘ

[1] Nazarbayev University, Physics Department, 010000, Nur-Sultan, Kazakhstan
[2] National Laboratory Astana, Nazarbayev University, 010000, Nur-Sultan, Kazakhstan

E-mail: aidar.kemelbay@nu.edu.kz

CrossMark

Abstract

Silver nanowire (AgNW) networks have attracted particular attention as transparent conductive films (TCF) due to their high conductivity, flexibility, transparency, and large scale processing compatible synthesis. As-prepared AgNW percolating networks typically suffer from high contact resistance, requiring additional post-synthetic processing. In this report, large area irradiation with 200 ns short intense pulsed ion beam (IPIB) was used to anneal and enhance the conductivity of AgNW network, deposited on temperature-sensitive polyethylene terephthalate (PET) substrate. A TCF sheet resistance shows irradiation dose dependence, decreasing by four orders of magnitude and reaching a value of 70 Ω/sq without damaging the polymer substrate, which retained a transparency of 94%. The IPIB irradiation fused AgNW network into the PET substrate, resulting in a great adhesion enhancement. Heat transfer simulations show that the heat originates at the near-surface layer of the TCF and lasts an ultra-short period of time. Obtained experimental and simulation results indicate that the irradiation with IPIBs opens new perspectives in the low-temperature annealing of nanomaterials deposited on temperature-sensitive substrates.

Supplementary material for this article is available online

(Some figures may appear in colour only in the online journal)

1. Introduction

Silver nanowires (AgNWs) based transparent conductive films (TCFs) are promising for application in flexible electronics due to their high electrical conductivity, mechanical flexibility, simple and cheap liquid phase synthesis [1–7]. AgNWs have been successfully implemented in transparent heaters, touch panels, flexible displays, fuel cells, solar cells, as electromagnetic interference shielding, current collectors and in other devices [8–14]. Various methods of AgNWs synthesis have been developed, among which, a polyol synthesis is one the most widely used ones [2, 7]. The method is technologically simple, inexpensive, and compatible with

drop-casting, dip-coating, spin-coating, rod-coating and other cost-effective deposition techniques [1, 11]. After the polyol synthesis, AgNWs are typically covered with a thin poly-vinylpyrrolidone (PVP) dielectric layer, which hinders the current flow at the contact points of the AgNWs in a TCF.

There are several important considerations for AgNWs-based TCFs fabrication and integration into flexible devices: (1) high electrical conductivity, which can be hindered by high contact resistance between the NWs in as-prepared networks; (2) adhesion, limited by weak interaction of AgNWs with substrate; and (3) long-term stability, which suffers from the reaction of silver with oxygen and sulfur, in the air. Therefore, to improve the properties of AgNWs-based TCFs, an additional post-deposition processing is usually required. This step should not degrade the optoelectronic and mechanical properties of both NW and substrate.

Various solutions have been proposed to improve the conductivity of AgNW percolating networks, with many efforts being put into the development of a nano-welding process [15]. The nano-welding was performed with liquid phase modifications or by using heat, light, and charged particles. The former utilizes capillary force [16] or chemical reaction [17] driven self-limiting, room temperature, large-scale fabrication compatible nano-welding. However, these methods limit the substrate choice due to the hydrophilicity and chemical stability requirements. Heating using conventional ovens, hotplates or rapid thermal annealing typically requires temperature in the range between 200 °C and 300 °C [18, 19], making them incompatible with temperature-sensitive polymer substrates and cannot be used for flexible electronics fabrication.

On the other hand, light-induced annealing, performed using lasers [20, 21], flash lamps [22] and sunlight [23] is local and rapid enough to be used with polymer substrates. The approach relies on plasmon resonance, originating at the junctions of NWs, resulting in a local heat generation and AgNWs nano-welding, without affecting the substrate. A lLaser-based annealing was also shown to be an effective technique for nano-welding of other metallic [24, 25] and semiconducting [26, 27] NWs. However, the light-induced annealing may result in the temperature variations due to light-specific physical phenomena, such as a highly material-dependent absorption, interference, and hot corner effects, which become more pronounced with ever-increasing geometrical and structural complexity of devices [28–30]. Additionally, the laser-based annealing requires extensive raster scanning, significantly increasing the processing time.

Charged particle beams, particularly electrons, also proved to be capable of AgNWs nano-welding and improving the optoelectronic properties of TCFs [31, 32]. The irradiation with ion beams was also shown to be promising, for which proton, copper, and carbon ions were used [33, 34]. It was argued that the welding occurs due to non-thermal effects, such as ion tracks formation and collision cascade diffusion processes. For continuous electron and ion beams, the heating is typically minimal due to the low current density of the techniques, which requires an ion fluence (dose) of 10^{15} ions cm^{-2} and higher. This increases the processing time

and makes the irradiation with continuous beams unfavorable for large scale fabrication.

In this work, the irradiation with intense (i.e. high-current density) pulsed ion beam (IPIBs) is used to enhance the conductivity of AgNW percolating network, deposited on top of the temperature-sensitive polyethylene terephthalate (PET) substrate. In the context of beam-matter interaction, there is an important difference between the irradiation with low current density continuous beams (μA cm^{-2}), discussed above, and high-intensity IPIBs (tens of A cm^{-2} and higher): the same number of particles is being delivered to the sample within significantly lower amount of time (min/hours versus nanoseconds) [35, 36]. As a result, the IPIB irradiation is accompanied with an enormous, but very short-lasting heat generation, restrained in the top few micrometers, while keeping the bulk of the substrate at low temperature.

2. Materials and methods

2.1. Synthesis of AgNWs

Silver nitrate (AgNO3, 99.8%), poly-vinyl pyrrolidone (PVP, MW = 360000), sodium chloride (NaCl, 99.5%), potassium bromide (KBr, 99%), ethylene glycol (EG, 99.0%) were purchased from Sigma-Aldrich. All reagents were used as received, without any further purification.

AgNWs were synthesized using a modified polyol method specially developed in our group. Firstly, 0.4 g of PVP was added to 75 ml of EG in a 100 ml conical flask. PVP was completely dissolved in EG by agitating the mixture using a magnetic stirrer (500 rpm), at 130 °C in 30 min. The resulting solution was transferred to a different hotplate with magnetic stirrer, preset to room-temperature and was cooled down to 20 °C, while stirring at 500 rpm. After that, 0.5 g of AgNO$_3$ powder was added to the solution, completely dissolved in 10 min at room-temperature, while stirring at 500 rpm. It is important to note that if the temperature of the solution before adding the AgNO$_3$ powder is above 30 °C, Ag gets oxidized and the solution becomes darker, resulting in the final product mostly consisting of Ag nanoparticles.

NaCl and KBr solution in EG was prepared in a separate vial by dissolving 0.1 g of NaCl and 0.015 g of KBr in 20 ml of EG, assisted with the ultrasonication. Next, 200 μl of NaCl and KBr solution in EG was added to AgNO$_3$ and PVP solution and stirred for two minutes at room-temperature. The resulting mixture was transferred to the hot-plate pre-heated to 130 °C (without oil bath) and was stirred with 500 rpm. After 10 min the stirring was turned off and the mixture was left without agitation for AgNWs to grow at 130 °C for 5 h. Finally, the suspension was cooled down to room temperature, subsequently washed in ethanol three times by centrifugation at 2000 rpm for 10 min. After the centrifugation, a small amount of large visible agglomerates of AgNWs were observed in the suspension. To remove the agglomerates, the solution was filtered through several layers of nylon fabric.
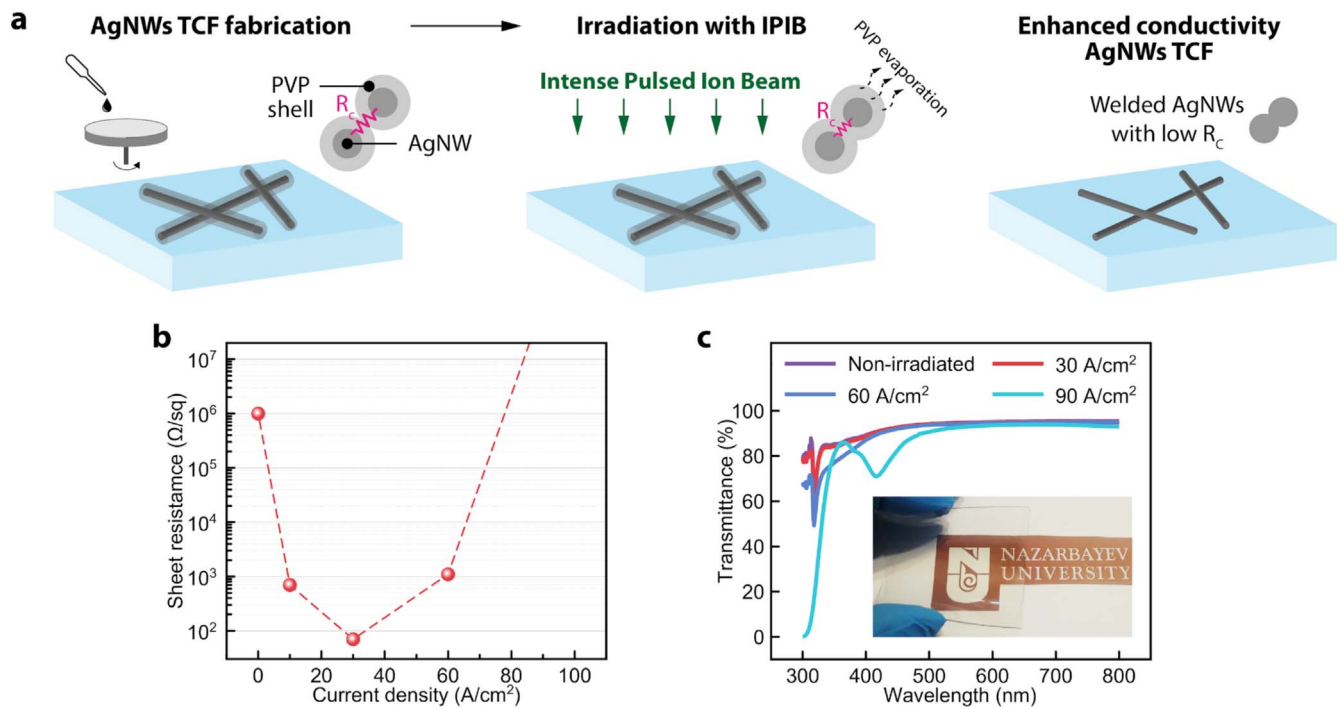
Figure 1. (a) Schematic illustration of AgNW-based TCFs fabrication and irradiation with IPIB. (b) The sheet resistance evolution as a function of the IPIB current density, demonstrating the conductivity improvement by four orders of magnitude. (c) Optical transmittance dependence on the beam current density, confirming the highly transparent nature of TCFs after the irradiation.

After the filtration, no visible agglomerations were found in the dispersion, which was further used in experiments. The PVP layer improves NWs dispersion in solution and prevents agglomeration due to steric repulsion. The dimensions of synthesized AgNWs were routinely estimated by obtaining SEM images from multiple spots (at least 5) across the sample and analyzing the images with the ImageJ software. The average diameter and length were 55 ± 6 nm and 20–40 μm, respectively.

2.2. Fabrication of flexible TCFs

The PET films (5×5 cm^2 with a thickness of 500 μm) were used as substrates for AgNW TCFs fabrication. The PET was fixed to a rigid substrate holder using double-sided conductive tape during TCF fabrication, irradiation and characterization steps, where applicable. Firstly, the PET substrates were cleaned using sonication in DI-water, followed by sonication in ethanol, each for 10 min. Next, 2 ml of AgNWs dispersed in ethanol was dropped on the PET film, which was enough to fully cover the surface of the substrate, followed by spin-coating at 1000 rpm for 2 min. In 2 min most of the ethanol evaporated from the substrate and AgNWs uniformly covered the PET substrate without the coffee-stain effect. Next, as-prepared TCFs were dried in the oven at 50 °C for 20 min to ensure complete ethanol removal. The coating procedure was repeated four times to increase the density of AgNWs. Subsequently, the AgNW networks on the PET substrate were treated by one pulse of IPIB with different beam current densities at the Innovative Nazarbayev University's Research Accelerator (INURA)

facility [35]. The obtained samples were irradiated with a single IPIB pulse with a total duration of 200 ns, consisting of protons with a peak kinetic energy of 300 keV. For uniform irradiation, the beam spot size was kept larger than the size of samples in all experiments. The beam current density was varied in the range from 10 to 90 A cm^{-2}, which corresponded to a fluence from $3 \cdot 10^{12}$ to $3 \cdot 10^{13}$ ions cm^{-2}, respectively. A corresponding schematic illustration is shown in figure 1(a).

2.3. Characterization

The shape and size of AgNWs before and after irradiation with IPIB were studied using the Carl Zeiss Crossbeam 540 scanning electron microscope (SEM). Structure and crystallinity of AgNWs were analyzed with the Rigaku SmartLab x-ray diffraction (XRD) system equipped with a Cu Kα radiation source. Transmittance and absorbance spectra of TCFs were measured with the Perkin Elmer UV–vis–NIR spectrophotometer. The sheet resistance of TCFs was measured using the Jandel RM3000+ four-probe measurement system. Atomic force microscopy (AFM) measurements were performed on the AIST-NT SmartSPM 1000 microscope. Optical images were obtained with the ZEISS Axioscope 5 microscope. All measurements were performed at Nazarbayev University Core Facility. The adhesive tape test was performed by attaching a 3 M Scotch tape, firmly pressing it against the TCF and slowly peeling it off in the same way for all samples.
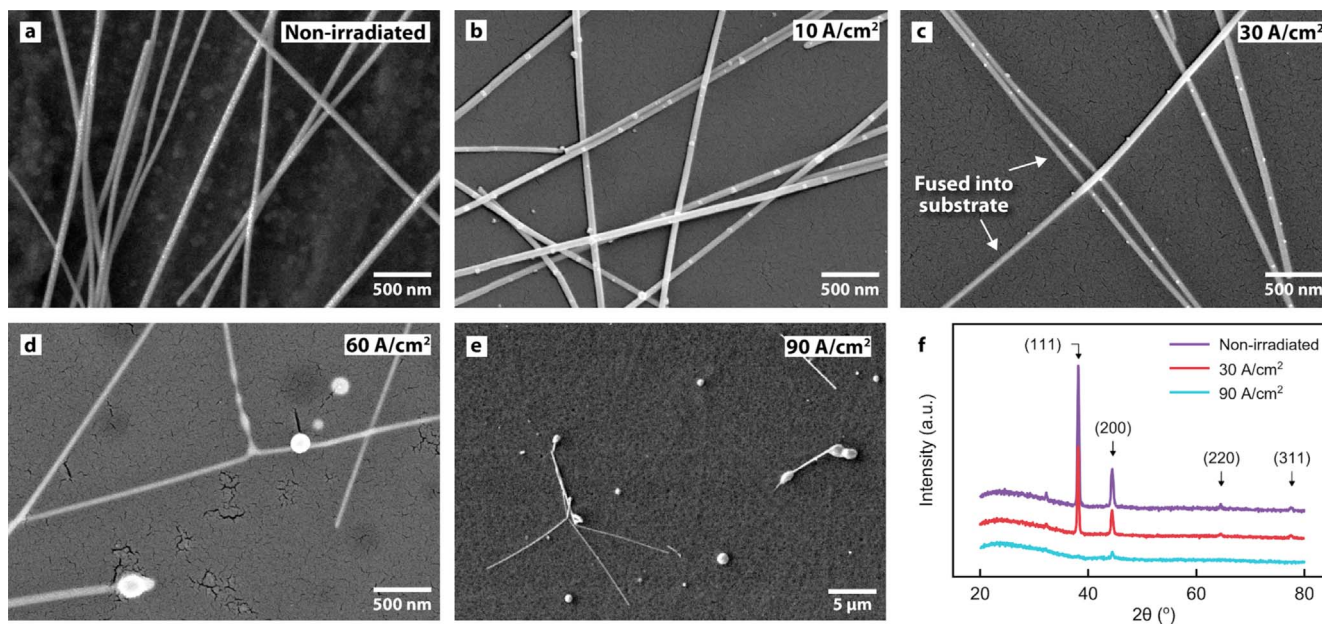
Figure 2. (a) SEM images of AgNWs on PET substrate before; and (b)–(e) after the irradiation with a beam current density of (b) 10 A cm^{-2}, (c) 30 A cm^{-2}, (d) 60 A cm^{-2} and (e) 90 A cm^{-2}. (f) XRD measurements before and after the irradiation.

3. Experimental results

3.1. Electrical and optical properties of the AgNW networks irradiated with IPIB

Figure 1(b) shows the TCF sheet resistance measurement results before and after the irradiation. The as-prepared AgNW percolating network shows a high sheet resistance in the order of 10^6 Ω/sq due to the high contact resistance between AgNWs covered with the PVP. After the irradiation by IPIB with a beam current density of $j = 10$ A cm^{-2} the sheet resistance decreased to 600 Ω/sq, further decreasing to 70 Ω/sq at $j = 30$ A cm^{-2}. Increasing the beam current density to 60 A cm^{-2}, increased the sheet resistance of AgNW TCF to 10^3 Ω/sq. After the irradiation with a beam current density of 90 A cm^{-2}, the AgNW network becomes non-conductive. Thus, the electrical measurements showed that the sheet resistance can be modulated and optimized by changing the IPIB current density, decreasing by four orders of magnitude compared to as-prepared AgNWs after the irradiation with $j = 30$ A cm^{-2}.

The optical transmittance measurements revealed that the IPIB irradiation with a beam current density of up to 30 A cm^{-2} does not degrade the transmittance of the TCF in the visible range and slightly improves it in the ultraviolet range (figure 1(c)). The transmittance at 550 nm remained at 94%. The TCFs show a typical strong absorption band at 320 nm and a weaker one at 380 nm that correspond to the diameter-dependent quadrupole resonance excitation mode and transverse plasmon resonance of AgNWs, respectively [37–39]. Increasing the beam current density to 60 A cm^{-2} only slightly changed the transmittance, mostly in the UV-region, whereas after the irradiation with a current density of 90 A cm^{-2} an additional wide absorption band at 390–430 nm emerged. This band can be attributed to the formation of Ag nanoparticles [39]. The inset in figure 1(c) shows a photograph of the fabricated AgNWs on PET, irradiated with a current density of 30 A cm^{-2} and placed on top of the Nazarbayev University logo, demonstrating the high transparency of the TCF.

To comparatively evaluate the performance of the TCF with the highest conductivity, a commonly used figure of merit (FOM) [40] was calculated using the following equation: FOM $= (T/100)^{10}/R_{sh}$, where, T is the transmittance (%) and R_{sh} is the sheet resistance (Ω/sq). Using the obtained values for the sheet resistance (70 Ω/sq) and transmittance (94%) of the sample after the irradiation with a current density of 30 A cm^{-2}, a FOM of 7.7×10^{-3} was obtained, which is better or comparable with the FOMs reported for the widely used ITO films [1]. However, unlike AgNWs, the ITO suffers from brittleness and inability to withstand strain higher than 1%, which makes it unsuitable for many flexible device applications [41]. The obtained FOM is also comparable with those reported for other nanowires [1], although the electrical conductivity can be further improved by optimizing the synthesis parameters.

3.2. Morphology and crystallinity of the AgNW networks irradiated with IPIB

The morphology of AgNW networks on PET after the irradiation was further studied using the SEM. Figures 2(a)–(e) shows the regions of as-prepared and irradiated AgNWs, representative for entire samples with an area of 25 cm^2. After the irradiation with pulsed proton beam with a current density of 10 A cm^{-2}, small debris appear that we interpret as PVP residues formed as a result of PVP redistribution (figure 2(b)). Increasing the current density to 30 A cm^{-2} further decomposed the PVP with only small residues observed afterwards. A slight local flattening of NWs at the junctions, together with
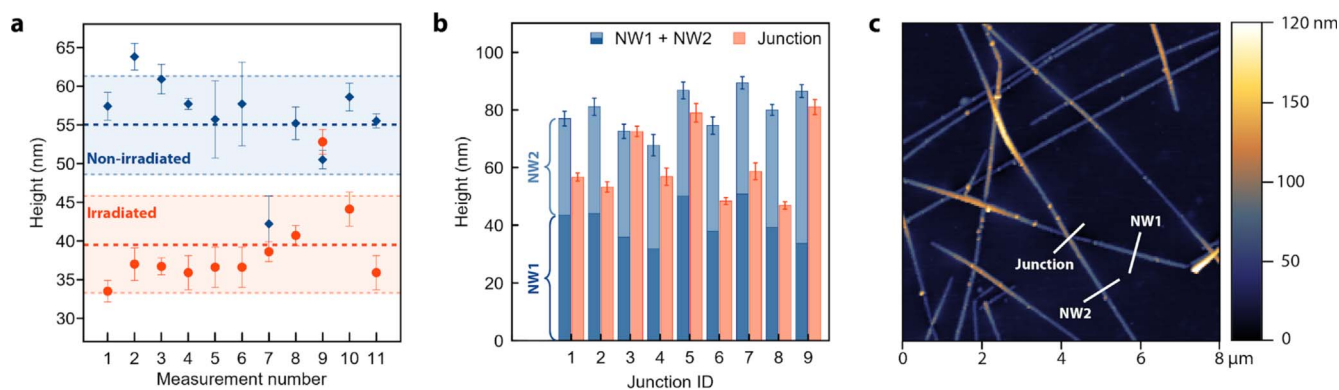
Figure 3. (a) A comparison between the heights of randomly selected AgNWs before and after irradiation with $j = 30 \, \text{A cm}^{-2}$, indicating a significant difference that can be attributed to the fusion of AgNWs into PET upon irradiation. (b) The height of various regions on the irradiated AgNWs, showing that the stacked height (sum of heights) of NWs (labelled as 'NW1 + NW2') is higher than the measured height of the junction that these NWs form (labelled as 'Junction'), suggesting their nano-welding. (c) A representative AFM image of AgNW percolating network with solid lines demonstrating how analysis in (b) was performed.

a significantly improved sheet resistance, suggests that the nano-welding of AgNWs occurs as another mechanism behind the contact resistance improvement. Further increase of the beam current density to $60 \, \text{A cm}^{-2}$ resulted in Ag nanobeads formation and a more pronounced fusion of the AgNWs into the PET. The former can be explained by the Rayleigh instability induced transformations that result in metal NWs breaking up (melting) into nanoparticles under annealing at high temperatures. After the irradiation with a current density of $90 \, \text{A cm}^{-2}$, the percolation network becomes completely discontinuous with more pronounced nanobeads formation, which might be of interest for plasmonic applications [42]. The evolution of the AgNWs morphology at different current density values explains and perfectly matches with the sheet resistance evolution, as well as with the changes observed with the optical transmittance measurements. The obtained results show that the irradiation with a single IPIB pulse of 200 ns duration can be used to enhance the AgNW network conductivity through the heat-induced PVP removal and nano-welding, while simultaneously fusing the network into the PET substrate.

XRD measurements were performed to study the crystallinity of the AgNWs after the irradiation with the different current densities (figure 2(f)). The XRD pattern of as-prepared NWs revealed their face-centered cubic [38] structure with a lattice parameter of $a = 0.408 \, \text{nm}$. After the irradiation with a current density of $30 \, \text{A cm}^{-2}$, the intensities of (111), (200), (220) and (311) peaks slightly decreased, without any detectable shift and change in the lattice parameter, suggesting that the degree of crystallinity reduced only slightly. The XRD spectra of the AgNWs irradiated with a current density of $90 \, \text{A cm}^{-2}$ showed almost no peaks, indicating complete amorphization.

AFM was used to evaluate the topography of non-irradiated AgNWs, and the TCF with the highest conductivity irradiated with a beam current density of $30 \, \text{A cm}^{-2}$. Figure 3(a) compares the heights of non-irradiated and irradiated AgNWs, as well as indicates their average heights (thick dashed lines) and the corresponding standard deviations (thin dashed lines). The average height of non-irradiated

NWs was measured to be $55 \pm 6 \, \text{nm}$, which matches the NW diameters estimated with the SEM. After the irradiation with a beam current density $30 \, \text{A cm}^{-2}$ the average height was reduced to $39 \pm 5 \, \text{nm}$ with respect to the PET substrate. The observed difference, together with the SEM results, show that the PVP layer was removed and that the NWs were partially fused into the polymer substrate. The latter is advantageous for the improvement of the mechanical stability of the percolating network. Figure 3(b) compares the height of AgNWs junction after the irradiation (labelled as 'Junction') with the sum of the heights of two NWs that form it (labelled as 'NW1' and 'NW2'). Solid white lines in figure 3(c) demonstrate how these height profiles were extracted. The analysis shows that the calculated algebraic sum 'NW1 + NW2' is in most cases higher than the height of the junction that they form. The obtained AFM results match with the SEM observations and correlate well with the previously discussed improvement of the sheet resistance, together pointing towards AgNWs welding and fusion into the PET substrate.

3.3. Mechanical flexibility and adhesive properties of the AgNW network after IPIB irradiation

The observed AgNWs fusion into PET and nano-welding should result in mechanical stability improvement of the network. To confirm it, the TCF irradiated with a beam current density $30 \, \text{A cm}^{-2}$ was tested by cycling bending. Figure 4(a) shows that the relative resistivity change was within 4% while applying 200 bending cycles, demonstrating excellent durability of the TCF. To further confirm the latter, the adhesive tape test was performed by firmly pressing the tape onto the right half of samples and slowly peeling it off. Figure 4(b) shows the corresponding optical microscopy images, obtained for the non-irradiated and irradiated samples after the tape removal. The non-irradiated AgNWs showed poor adhesion to the substrate with many NWs removed after peeling off of the adhesive tape. In contrast, the irradiated samples demonstrated excellent AgNWs adhesion to the PET substrate, without the visual change in the NWs areal density after the testing. Bending cycling and adhesive tape tests
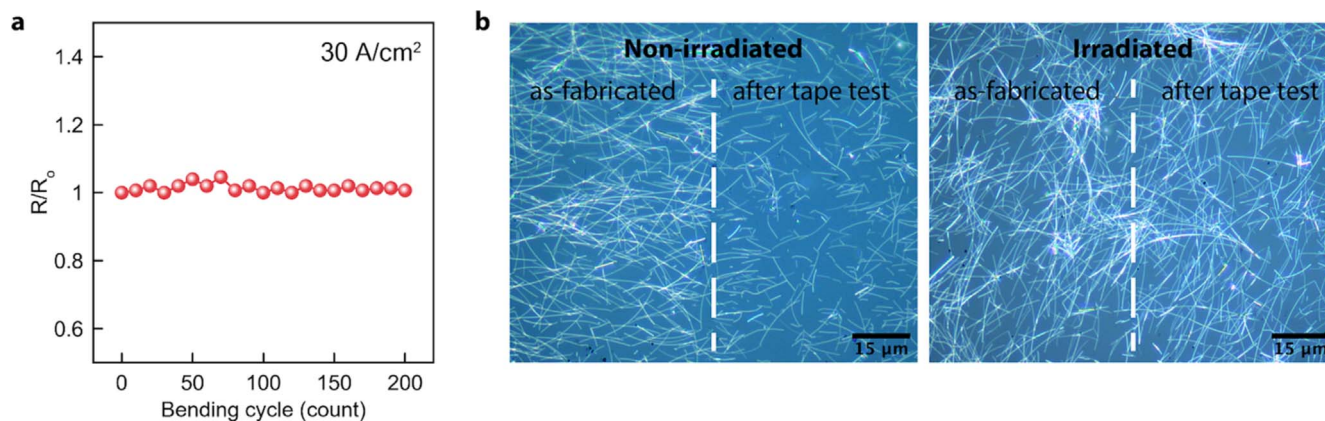
Figure 4. Mechanical stability of AgNW-based TCF irradiated with $j = 30$ A cm^{-2}, tested using (a) bending cycling tests, showing no degradation of the sheet resistance; and (b) adhesive tape test revealing high mechanical stability of the irradiated sample.

support the SEM and AFM results, confirming the fusion of AgNWs into the polymer substrate, which improved their mechanical stability.

3.4. The simulation of heat transfer in AgNW-based TFT upon IPIB irradiation

The Stopping and Range of Ions in Matter (SRIM) software [43] was used to gain the information about protons interaction with a target, consisting of a thin layer of Ag (110 nm) on PET. Irradiation parameters, consistent with our experiments, were used for simulations. The average penetration depth of a proton beam with a kinetic energy of 300 keV was calculated to be 3.5 μm (figure S1(a) (available online at stacks.iop.org/NANO/32/145706/mmedia)), which suggests that only the surface layer of the sample interacts with the beam and that no IPIB-induced doping of AgNWs should be expected. For protons with energies of several hundreds keV, the electronic stopping dominates over the nuclear stopping, indicating that most of the kinetic energy of incoming protons is converted into heat rather than recoil atoms. The latter becomes more pronounced deeper inside the PET substrate, avoiding the sputtering of AgNWs. While the discussed energy transfer mechanism is true for both low current density continuous beams and high current density IPIBs, the heat generated by the latter is significantly higher due to ultra-short pulse duration, so the near-surface layer of the target does not have time to cool down during the pulse. The SRIM simulation revealed that the collision of protons with the target induces Ag vacancies with a concentration of 10^{17}–10^{18} cm^{-3} for the beam current density range used in this study (figure S1(b)). We presume that the actual intrinsic defect concentration should be significantly lower (if any), since the created defects are annealed out at high temperatures caused by a high-current density of IPIB.

Since the direct temperature measurement with nanosecond resolution is a challenging task, the IPIB-induced thermal annealing was modeled using the one-dimensional time-dependent finite element method in COMSOL Multiphysics. Proton beam energy loss, calculated with the SRIM and demonstrated in figure S1(c), together with the ion beam

current density time dependence profile, measured with the accelerator's Faraday cup detector, were used to calculate the time- and depth-dependent ion beam power density transferred into the material [44], which was used as a heat source in simulations. The initial temperature across the sample was set to $T_0 = 293$ K. At the substrate-to-vacuum interface we used radiation boundary conditions, describing the radiating heat transfer governed by the Stefan–Boltzmann law: $J = \varepsilon\sigma(T^4 - T_0^4)$, where J is the surface-to-ambient radiative flux, ε is the emissivity, σ is the Stefan–Boltzmann constant.

Figure 5(a) shows the obtained temperature evolution for the first 2 μs for two cases: (1) 55 nm thick Ag layer; and (2) bilayer Ag with a total thickness of 110 nm. The first case represents an individual AgNW, while the second case represents a two-nanowire junction. The PET (substrate) thickness was set to 500 μm. The PVP thickness was not taken into account since it is too small to noticeably contribute to the heat transfer process. The inset in figure 5(a) demonstrates the temperature evolution for a 100 ms long period.

Simulations revealed that within the first ~200 ns, the temperature rockets from the room temperature to 735 °C and 856 °C for an individual and bilayer Ag, respectively. Both profiles demonstrate that the annealing temperature reaches values high enough for PVP evaporation and Ag softening or melting. The annealing thermal budget of the Ag bilayer is noticeably higher than that of the individual Ag layer, which is expected for a thicker metallic layer, and can be explained by higher ion energy loss in Ag compared to PET (figure S1(c)). The obtained simulation results suggest that the local temperature at AgNWs junctions is the highest, explaining their heat-induced local flattening, observed with the SEM.

Figures 5(b)–(c) show the temperature evolution as a function of the sample depth. The simulation shows that the heat originates during the first 200 ns (figure 5(b)), within the top 3.5 μm of the sample, which corresponds to the proton penetration depth (compare with figure S1(a)). Due to a higher energy loss in Ag, compared to PET, the former heats more, reaching a temperature of 850 °C. A second wide peak can be observed at around 3 μm, where most protons stop, corresponding to the Bragg peak. After the irradiation stops
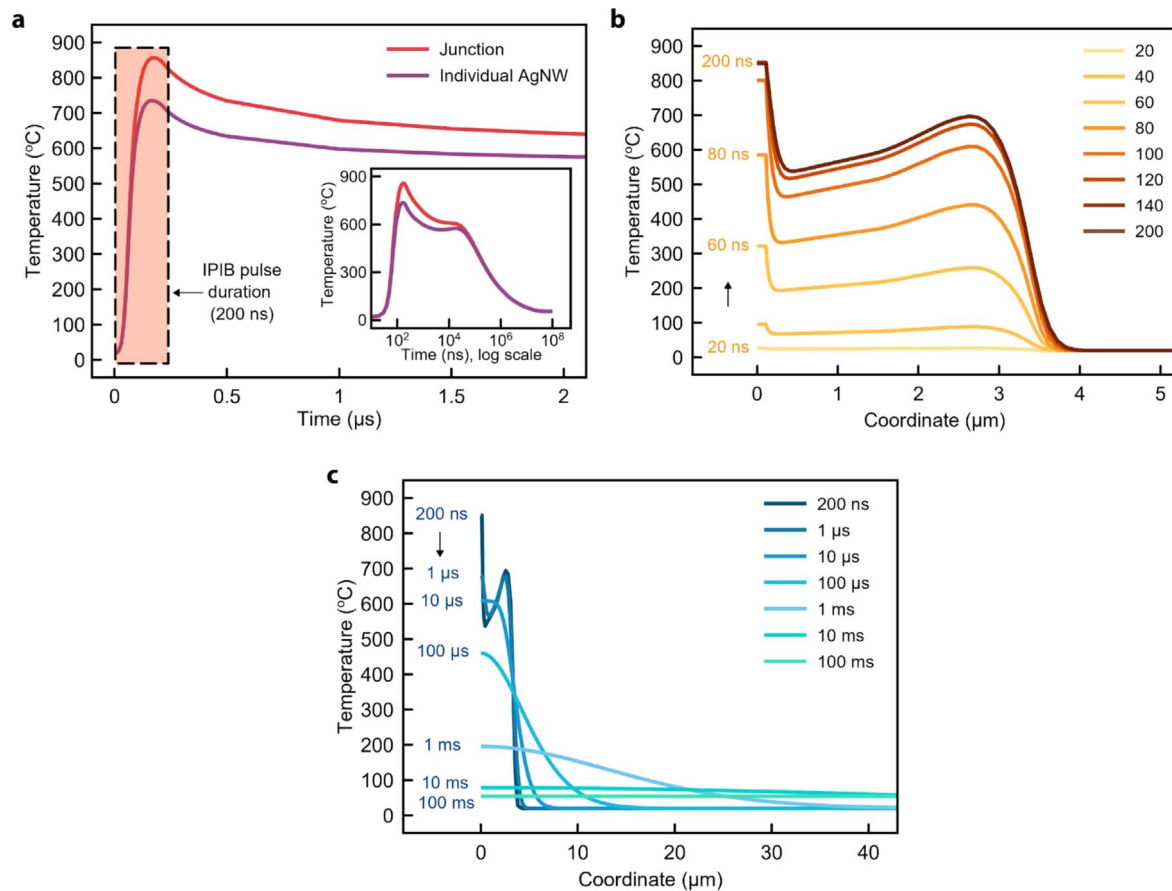
Figure 5. (a) IPIB-induced temperature evolution as a function of time in structures consisting of 55 and 110 nm thick Ag on 500 μm thick PET, representing individual AgNW and NWs junction, respectively. (b) Temperature evolution as a function of depth in 110 nm thick Ag on PET structure for the first 200 ns, i.e. during the irradiation; and (b) after the irradiation in the 200 ns − 100 ms time range.

(figure 5(c)), the temperature across the first 3.5 μm starts to stabilize, reaching equilibrium within $\sim$10 μs. Simultaneously, heat starts to propagate deeper into the bulk of the PET. Within a sub-1 ms period of time, the temperature across the entire sample becomes below 260 °C, which corresponds to the melting point of the PET. Although the temperatures obtained in the simulation are much higher at first, it was shown experimentally by other authors that polymers can withstand high temperatures if the annealing is rapid and local [45, 46]. Our simulations show that the heating and cooling rates are in the order of 10^8–10^9 °C s^{-1} and 10^3–10^8 °C s^{-1}, respectively. Such high rates, together with the surface annealing, are important to avoid the thermal degradation of polymer substrates.

4. Discussion

The IPIB technology was initially developed in late 1970s for the high-energy-density physics experiments, later finding new applications to modify the near-surface layer of bulk materials, such as metals, alloys, ceramics and films [47, 48], while the effect of IPIBs on nanomaterials remains an underexplored field. In this work we demonstrated that the irradiation with IPIBs can be used to improve the conductivity

of AgNW network deposited on PET substrate. We believe that this technique can be extended to other nanomaterials, where low-temperature processing is required. Table 1 continues the discussion provided in the introduction section and compares various techniques with the focus on the annealing of nanomaterials deposited on temperature-sensitive polymer substrates. The required low-thermal budget annealing can be achieved using laser, flash lamp and charged particles based treatment, each having unique capabilities and limitations. For example, laser processing offers local temperature increase and welding at NWs junctions caused by plasmonic effects, while the surrounding parts remain at considerably lower temperatures. Continuous ion and electron beam irradiation induce AgNWs welding mostly through non-thermal effects. Compared to these techniques, the irradiation with IPIBs heats the entire surface several microns deep for a very short period of time and can be used as an alternative method to improve the conductivity of AgNW network on flexible substrates.

The irradiation with IPIBs is a highly tunable process. The demonstrated extremely high heating and cooling rates can be increased or decreased by changing the beam current density, pulse duration, sample composition (e.g. substrate), etc. The beam penetration depth can be varied by adjusting the ion kinetic energy or by choosing different ion species

Table 1. A comparison of techniques used for the annealing of nanomaterials deposited on temperature-sensitive substrates.

Annealing method	Thermal budget	Advantages	Disadvantages	References
Hotplates, oven, IR RTA	Very high	Widely available, technologically simple, cheap	High-temperature, incompatible with polymer substrates	[18, 19]
Laser (pulsed and continuous)	Very low	Local, low-temperature, sub-nanosecond heating rate, plasmon welding is possible, compatible with polymer substrates, microscale patterning	Long processing time, material dependent absorption, interference, high power consumption	[15, 20, 21]
Flash lamp	Low	Low-temperature, sub-second heating rate, plasmon welding is possible, roll-to-roll processing and polymer substrate compatible,	Material dependent absorption, interference, high power consumption	[22, 23, 45, 46]
Continuous ion and electron beam	Extra low	Mostly non-thermal, compatible with polymer substrates	Long processing time, high fluence, defects creation, requires complicated radiation protection	[31, 33, 34, 49]
Pulsed ion and electron beams (non-focused)	Very low	Near-surface, sub-microsecond heating rate, roll-to-roll processing compatible, very low power consumption, (possible) defects annealing	Requires simple local radiation protection, irradiation with ions require vacuum in sample chamber	[32, 50], this work

(heavier/lighter), so that the energy loss profile in figure S1(a) can be shifted closer to the surface or deeper inside the sample, as well as widened or narrowed, depending on the application. Such a tunable interaction volume, translating into annealing volume, together with tunable heating and cooling rates are important for controllable modification of nanomaterials, allowing to avoid the thermal degradation of polymer substrates. Additionally, ultra-short large-area IPIB pulse makes the technique roll-to-roll process compatible. Industrial accelerators are capable of processing with a speed of higher than 4000 cm^2 per hour and a total energy consumption of less than 10 kW·hour. On the other hand, vacuum required for the operation of an ion beam accelerator, may limit the choice of materials, as well as increase the processing time and complicate the fabrication process. Nevertheless, integration of vacuum chambers with roll-to-roll fabrication systems is well-established, for example, in large scale track membranes fabrication using cyclotrons [51]. Particle accelerators draw special attention from the radiation safety point of view, however, the radiation exposure from an IPIB accelerator does not exceed the natural background radiation level, if a very simple and local protection is implemented.

5. Conclusion

Summarizing, a large-area IPIB irradiation improved the contact resistance of AgNW percolating network and fused it into the PET substrate—all with one 200 ns short irradiation pulse. The irradiation resulted in four orders of magnitude decrease of the sheet resistance from 10^6 Ω/sq to 70 Ω/sq, while the fusion significantly improved mechanical stability of the TCF. The morphological modifications occurred without the changes in AgNWs crystallinity and degradation of polymer substrate transmittance, which remained at 94%. The heat transfer simulations revealed that the IPIB irradiation results in a local near-surface annealing with a very high heating and cooling rates. The proposed technique will inspire more applications, where large-scale low-temperature annealing of nanomaterials on temperature-sensitive substrates is required.

Acknowledgments

Conflict of interest

The authors declare no conflict of interests.

ORCID iDs

Aidar Kemelbay ⓘ https://orcid.org/0000-0002-3321-1483
Alexander Tikhonov ⓘ https://orcid.org/0000-0001-6302-6599

References

[1] Li W *et al* 2020 Recent progress in silver nanowire networks for flexible organic electronics *J. Mater. Chem.* C **8** 4636–74
[2] Sun Y and Xia Y 2002 Large-scale synthesis of uniform silver nanowires through a soft, self-seeding, polyol process *Adv. Mater.* **14** 833
[3] Zhan K, Su R, Bai S, Yu Z, Cheng N, Wang C, Xu S, Liu W, Guo S and Zhao X-Z 2016 One-pot stirring-free synthesis of silver nanowires with tunable lengths and diameters via a Fe³⁺ & Cl⁻ co-mediated polyol method and their application as transparent conductive films *Nanoscale* **8** 18121–33
[4] Sun X M and Li Y D 2005 Cylindrical silver nanowires: preparation, structure, and optical properties *Adv. Mater.* **17** 2626–30
[5] Lee E-J, Kim Y-H, Hwang D K, Choi W K and Kim J-Y 2016 Synthesis and optoelectronic characteristics of 20 nm diameter silver nanowires for highly transparent electrode films *RSC Adv.* **6** 11702–10
[6] Liu Y, Chen Y, Shi R, Cao L, Wang Z, Sun T, Lin J, Liu J and Huang W 2017 High-yield and rapid synthesis of ultrathin silver nanowires for low-haze transparent conductors *RSC Adv.* **7** 4891–5
[7] Li B, Ye S, Stewart I E, Alvarez S and Wiley B J 2015 Synthesis and purification of silver nanowires to make conducting films with a transmittance of 99% *Nano Lett.* **15** 6722–6
[8] Ding Z, Stoichkov V, Horie M, Brousseau E and Kettle J 2016 Spray coated silver nanowires as transparent electrodes in OPVs for building integrated photovoltaics applications *Sol. Energy Mater. Sol. Cells* **157** 305–11
[9] Celle C, Mayousse C, Moreau E, Basti H, Carella A and Simonato J-P 2012 Highly flexible transparent film heaters based on random networks of silver nanowires *Nano Res.* **5** 427–33
[10] Leem D-S, Edwards A, Faist M, Nelson J, Bradley D D C and Mello J C D 2011 Efficient organic solar cells with solution-processed silver nanowire electrodes *Adv. Mater.* **23** 4371–5
[11] Pasquarelli R M, Ginley D S and O'hayre R 2011 Solution processing of transparent conductors: from flask to film *Chem. Soc. Rev.* **40** 5406
[12] Zeng L, Zhao T S and An L 2015 A high-performance supportless silver nanowire catalyst for anion exchange membrane fuel cells *J. Mater. Chem.* A **3** 1410–6
[13] Jung J, Lee H, Ha I, Cho H, Kim K K, Kwon J, Won P, Hong S and Ko S H 2017 Highly stretchable and transparent electromagnetic interference shielding film based on silver nanowire percolation network for wearable electronics applications *ACS Appl. Mater. Interfaces* **9** 44609–16
[14] Chang I, Park T, Lee J, Lee M H, Ko S H and Cha S W 2013 Bendable polymer electrolyte fuel cell using highly flexible Ag nanowire percolation network current collectors *J. Mater. Chem.* A **1** 8541
[15] Ding Y, Cui Y, Liu X, Liu G and Shan F 2020 Welded silver nanowire networks as high-performance transparent conductive electrodes: welding techniques and device applications *Appl. Mater. Today* **20** 100634
[16] Zhou X, Zhou Y, Ku J C, Zhang C and Mirkin C A 2014 Capillary force-driven, large-area alignment of multi-segmented nanowires *ACS Nano* **8** 1511–6

[17] Ge Y, Duan X, Zhang M, Mei L, Hu J, Hu W and Duan X 2017 Direct room temperature welding and chemical protection of silver nanowire thin films for high performance transparent conductors *J. Am. Chem. Soc.* **140** 193–9

[18] Kim C-L, Lee J-Y, Shin D-G, Yeo J-S and Kim D-E 2020 Mechanism of heat-induced fusion of silver nanowires *Sci. Rep.* **10** 9271

[19] Langley D P, Lagrange M, Giusti G, Jiménez C, Bréchet Y, Nguyen N D and Bellet D 2014 Metallic nanowire networks: effects of thermal annealing on electrical resistance *Nanoscale* **6** 13535–43

[20] Lee J, Lee P, Lee H, Lee D, Lee S S and Ko S H 2012 Very long Ag nanowire synthesis and its application in a highly transparent, conductive and flexible metal electrode touch panel *Nanoscale* **4** 6408–14

[21] Lee P, Lee J, Lee H, Yeo J, Hong S, Nam K H, Lee D, Lee S S and Ko S H 2012 Highly stretchable and highly conductive metal electrode by very long metal nanowire percolation network *Adv. Mater.* **24** 3326–32

[22] Park J H, Hwang G-T, Kim S, Seo J, Park H-J, Yu K, Kim T-S and Lee K J 2017 Flash-induced self-limited plasmonic welding of silver nanowire network for transparent flexible energy harvester *Adv. Mater.* **29** 1603473

[23] Kou P, Yang L, Chang C and He S 2017 Improved flexible transparent conductive electrodes based on silver nanowire networks by a simple sunlight illumination approach *Sci. Rep.* **7** 42052

[24] Han S *et al* 2014 Fast plasmonic laser nanowelding for a Cu-nanowire percolation network for flexible transparent conductors and stretchable electronics *Adv. Mater.* **26** 5808–14

[25] Park J H *et al* 2017 Plasmonic-tuned flash Cu nanowelding with ultrafast photochemical-reducing and interlocking on flexible plastics *Adv. Funct. Mater.* **27** 1701138

[26] Rickey K M, Nian Q, Zhang G, Chen L, Suslov S, Bhat S V, Wu Y, Cheng G J and Ruan X 2015 Welding of semiconductor nanowires by coupling laser-induced peening and localized heating *Sci. Rep.* **5** 16052

[27] Xing S, Lin L, Zou G, Duley W W, Liu L and Norman Zhou Y 2019 Two-photon absorption induced nanowelding for assembling ZnO nanowires with enhanced photoelectrical properties *Appl. Phys. Lett.* **115** 103101

[28] Gebel T, Rebohle L, Fendler R, Hentsch W, Skorupa W, Voelskow M, Anwand W and Yankov R A 2006 Millisecond annealing with flashlamps: tool and process challenges *2006 14th IEEE Int. Conf. on Advanced Thermal Processing of Semiconductors* (https://doi.org/10.1109/RTP.2006.367981)

[29] Lanzerath F, Buca D, Trinkaus H, Goryll M, Mantl S, Knoch J, Breuer U, Skorupa W and Ghyselen B 2008 Boron activation and diffusion in silicon and strained silicon-on-insulator by rapid thermal and flash lamp annealings *J. Appl. Phys.* **104** 044908

[30] Rebohle L, Prucnal S and Skorupa W 2016 A review of thermal processing in the subsecond range: semiconductors and beyond *Semicond. Sci. Technol.* **31** 103001

[31] Hong C-H, Oh S K, Kim T K, Cha Y-J, Kwak J S, Shin J-H, Ju B-K and Cheong W-S 2015 Electron beam irradiated silver nanowires for a highly transparent heater *Sci. Rep.* **5** 17716

[32] Kim J, Nam Y S, Song M H and Park H W 2016 Large pulsed electron beam welded percolation networks of silver nanowires for transparent and flexible electrodes *ACS Appl. Mater. Interfaces* **8** 20938–45

[33] Shehla H, Saira R, Ishaq A, Khan Y, Shahzad N, Maaza M and Javed I 2016 Ion beam irradiation-induced nano-welding of Ag nanowires *Micro Nano Lett.* **11** 34–7

[34] Bari B, Honey S, Morgan M, Ahmad I, Khan R, Muhammad A, Alamgir K, Naseem S and Malik M 2015 MeV carbon ion irradiation-induced changes in the electrical conductivity of silver nanowire networks *Curr. Appl. Phys.* **15** 642–7

[35] Kaikanov M *et al* 2016 An accelerator facility for WDM, HEDP, and HIF investigations in Nazarbayev University *J. Phys. Conf. Ser.* **717** 012099

[36] Bedin S, Ovchinnikov V, Remnev G, Makhin'ko F, Pavlov S, Gushchina N and Zagorskiy D 2018 Radiation stability of metal $Fe_{0.56}Ni_{0.44}$ nanowires exposed to powerful pulsed ion beams *Phys. Met. Metall.* **119** 44–51

[37] Bari B, Lee J, Jang T, Won P, Ko S H, Alamgir K, Arshad M and Guo L J 2016 Simple hydrothermal synthesis of very-long and thin silver nanowires and their application in high quality transparent electrodes *J. Mater. Chem.* A **4** 11365–71

[38] Lee J H, Lee P, Lee D, Lee S S and Ko S H 2012 Large-scale synthesis and characterization of very long silver nanowires via successive multistep growth *Cryst. Growth Des.* **12** 5598–605

[39] Sun Y, Gates B, Mayers B and Xia Y 2002 Crystalline silver nanowires by soft solution processing *Nano Lett.* **2** 165–8

[40] Haacke G 1976 New figure of merit for transparent conductors *J. Appl. Phys.* **47** 4086–9

[41] Kulkarni G U, Kiruthika S, Gupta R and Rao K 2015 Towards low cost materials and methods for transparent electrodes *Curr. Opin. Chem. Eng.* **8** 60–8

[42] Oh H, Lee J and Lee M 2018 Transformation of silver nanowires into nanoparticles by Rayleigh instability: comparison between laser irradiation and heat treatment *Appl. Surf. Sci.* **427** 65–73

[43] Ziegler J F, Ziegler M and Biersack J 2010 SRIM—the stopping and range of ions in matter (2010) *Nucl. Instrum. Methods Phys. Res.* B **268** 1818–23

[44] Yu X, Shen J, Qu M, Zhong H, Zhang J, Zhang Y, Yan S, Zhang G, Zhang X and Le X 2015 Distribution and evolution of thermal field formed by intense pulsed ion beam on thin metal target *Nucl. Instrum. Methods Phys. Res.* B **365** 225–9

[45] Niittynen J, Sowade E, Kang H, Baumann R R and Mäntysalo M 2015 Comparison of laser and intense pulsed light sintering (IPL) for inkjet-printed copper nanoparticle layers *Sci. Rep.* **5** 8832

[46] Daunis T B, Schroder K A and Hsu J W P 2020 Photonic curing of solution-deposited ZrO_2 dielectric on PEN: a path towards high-throughput processing of oxide electronics *npj Flexible Electron.* **4** 7

[47] Yu X *et al* 2020 Focusing of intense pulsed ion beam by magnetically insulated diode for material research *Surf. Coat. Technol.* **384** 125351

[48] Remnev G *et al* 1999 High intensity pulsed ion beam sources and their industrial applications *Surf. Coat. Technol.* **114** 206–12

[49] Ishaq A, Shehla H, Ali N Z, Akram W, Shakeel K, Diallo A, Shahzad N and Maaza M 2017 Improvement of optical transmittance and electrical conductivity of silver nanowires by Cu ion beam irradiation *Mater. Res. Express* **4** 075055

[50] Kaikanov Marat, Amanzhulov Bauyrzhan, Demeuova Gulzat, Akhtanova Gulnur, Bozheyev Farabi, Kemelbay Aidar and Tikhonov Alexander 2020 Modification of silver nanowire coatings with intense pulsed ion beam for transparent heaters *Nanomaterials* **10** 2153

[51] Ferain E and Legras R 1993 Heavy ion tracks in polycarbonate. Comparison with a heavy ion irradiated model compound (diphenyl carbonate) *Nucl. Inst. Methods Phys. Res.* B **82** 539–48